2021-03-26

Analytical solution for flange/web distortional buckling of cold-formed steel beams with circular web perforations

Voudouris, Vlasios

10.1080/15376494.2021.1902594
Mechanics of Advanced Materials and Structures
Taylor & Francis

Accepted on March 26 2021 for the publication in the Journal of Mechanics of Advanced Materials and Structures

https://doi.org/10.1080/15376494.2021.1902594

Analytical solution for flange/web distortional buckling of cold-formed steel beams with circular web perforations

Nan-ting Yu[a,b], Boksun Kim[b], Xu-hao Huang[c], Wei-bin Yuan[a*], Rui Ye[a], Long Wu[a] and Jia-jie Le[a]

(a) College of Civil Engineering, Zhejiang University of Technology, Hangzhou 310023, PR China

(b) School of Engineering, Computing and Mathematics, University of Plymouth, Plymouth PL4 8AA, UK

(c) Faculty of Mechanical Engineering and Mechanics, Ningbo University, Ningbo 315211, China

Abstract:

Perforated cold-formed steel (PCFS) beams are increasingly used in constructional industry and become popular due to their advantages and economic benefit. Apart from the light weight, the openings in PCFS beams can also be used for services such as pipe utilities to release more building space. However, beams with web perforations may collapse as the result of web-distortional buckling or flange/web distortional buckling due to the web weakness caused by perforations. In this paper a study on the flange/web distortional buckling of PCFS beams is presented. An analytical solution to determine the critical stress of flange/web distortional buckling of PCFS beams is derived by using energy method. To demonstrate the analytical solution, finite element analysis is also carried out. The finite element analysis results show that the analytical solution provided can give good and reliable prediction for the flange/web distortional buckling of PCFS beams.

Keywords: Flange/web distortional buckling; PCFS beams; Openings; Energy method; Finite element analysis

1. Introduction

Cold-formed steel (CFS) is produced by the cold work instead of the heating processes. Compared with the hot-rolled steel, the CFS sections have lighter weight and higher yield strength due to the cold forming processes. It has grown to become competitive product in the building industry. The perforations of different shapes are usually punched in the middle of the webs to provide the space for the pipe utilities to pass through. The circular hole is the most popular type to minimize the effect of stress concentration. However, such openings make the sections more susceptible to elastic buckling. Similar to the CFS beams, the perforated cold-formed steel (PCFS) beams might also experience local, distortional and lateral-torsional buckling. The existing literatures mainly focused on numerical and experimental investigations of PCFS members. There is little information on developing the analytical approaches to predict the elastic buckling critical stress.

Moen and Schafer [1] presented simplified methods to determine the elastic buckling stress of PCFS members with slotted holes. The equation of global buckling stress was developed based on Rayleigh-Ritz energy solution, the principle of weighed average was used to cut down the cross-section properties. The local and distortional buckling stresses were generated by the finite strip analyses where the reduced thickness was utilised to modify the original models (no holes). It should be mentioned that Moen's approach for calculating the distortional buckling critical stress of PCFS members mainly depended on the numerical solution produced by CUFSM [2]. Later, Smith and Moen [3] applied this method to calculate the elastic buckling stress of steel pallet rack columns with perforation patterns. Liu and Chung [4] performed the finite element investigation to examine the structural characteristics of PCFS beams with various large web openings. Degtyarev and Degtyareva [5-6] extensively studied the elastic shear buckling characteristics and ultimate shear strength of PCFS beams with flat slotted openings by numerical simulations. After that, Pham et al. [7] proposed a practical model to acquire the shear yielding load with central square and circular web holes, which was validated using the DSM design equations.

For physical testing investigation, Moen and Schafer [8] conducted compression experiment on PCFS columns to study the connection between the buckling behaviour and ultimate strength. It was found that the slotted holes might change the half-wave lengths of local and distortional buckling modes, then altered the critical stress. The results of the test helped to widen the equations of direct strength method (DSM) to predict the ultimate strength of PCFS members. Crisan et al. [9] carried out the experiments on the buckling behaviour of PCFS compression members, the ultimate strength failed by local, distortional and interactive buckling were tested. Kulatunga and Macdonald [10-11] examined the effect of position and shape of the openings on the load capacity of PCFS columns, the experiment results were used to validate the finite element analysis. Lawson and Basta [12] performed single point load tests to investigate the deflection of PCFS beams. The formula for the additional deflections due to the circular web openings were derived. Recently, considerable amounts of research investigated the influence of edge-stiffened circular holes. For example, Uzzaman et al. [13-15] conducted the experimental investigation to explore the effects of edge-stiffened circular holes on the web crippling strength subjected to one-flange loading conditions or interior-two-flange loading conditions. Chen et al. [16-17] estimated the effects of hole spacing and column length on the load capacity of PCFS columns with edge-stiffened web openings; parametric study and simplified design equations were proposed. Later, they [18-19] investigated the moment capacity and axial strength of CFS beams and back-to-back CFS channels with edge-stiffened web holes, un-stiffened web holes and plain webs, respectively.

Yu et al. [20-22] discussed the distortional buckling behaviour of PCFS beams with central web openings subjected to pure bending and uniformly distributed loads. The simplified formula was proposed to calculate the distortional buckling critical stress. It was shown that the stress gradient might change the half-wave length of distortional buckling modes, and the critical stress of the beam under uniformly distributed loads was larger than that of the same beam under pure bending. For the beam under pure bending, the rotational spring stiffness in Hancock's model [23-24] and the vertical

spring stiffness in Eurocode 3 [25] were modified respectively based on the concept of equivalent width. It should be pointed out that the previous analytical method mainly focused on flange/lip distortional buckling, only the compressed flange-lip system was used to calculate the critical stress. Mousavi et al. [26] applied the improved element-free Galerkin with the finite strip to evaluate the buckling behaviour of CFS beams with web openings.

This paper describes an analytical solution for approximating the critical stresses of flange/web distortional buckling of PCFS beams when subjected to pure bending. A new model was derived based on the energy method and the eigenvalue equation was solved by using Rayleigh-Ritz method. To incorporate the influence of perforated web, the Hermite interpolating function was adopted. The finite element analyses were also carried out to check the accuracy of the analytical approach. The result showed that the proposed model can be used to predict the flange/web distortional stress of the PCFS beams accurately. Furthermore, the outcome of this research might provide the theoretical support for the design of PCFS beams.

2. Review of the distortional buckling modes of PCFS beams

The lip/flange distortional buckling was first revealed by Lau and Hancock [23-24]. It can be expressed as the rotation of the compressed lip and flange about the flange-web corner, meanwhile, the web will buckle at the same half-wave length. Fig.1 shows the buckling curves of the CFS sections in pure bending which was produced by CUFSM [2]. Normally the half-wave length of the lip/flange distortional buckling mode is two or three times larger than the dimension of the section (see point A in Fig.1). According to Hancock's model, other analytical models such as EN1993-1-3 model [25] and Li's [27] model were carried out to approximate the lip/flange distortional buckling critical stress of CFS members.

The flange/web distortional buckling (also called as lateral-distortional buckling) was defined by Rogers and Schuster [28]. They found that the compressed flange and lip would move laterally from the flange-web junction near the ultimate failure stage, the web would bend transversely at the same time. The half-wave length of the flange/web distortional buckling mode is longer than that of the flange/web distortional buckling mode (see point B in Fig.1) [29]. Later, Badawy Abu-Sena et al. [30] applied the energy method to investigate the interaction between the distortional buckling and the torsional-flexural buckling. More recently, Yuan et al. [31] put forward an analytical approach to illustrate the flange/web distortional buckling behaviour of partially restrained CFS purlins subjected to uplift loading. Zhu et al. [32-34] introduced a stiffened plate buckling model to calculate the flange/web distortional buckling critical stress of CFS members subjected to pure bending and compression.

For the PCFS beams, the openings can weaken the web flexural stiffness which leads to the loss of the rotational restraint to the compressed lip-flange system, resulting in the beams being more susceptible to distortional buckling. When the failure mode is controlled by the distortional buckling, the main influence of the opening is to reduce rotational stiffness, but has minimal impact on the half-wave length of the buckling mode [1]. Hence, the PCFS beams might experience the flange/web distortional buckling when the tension end of the web is laterally restrained (see Fig.2 (a)). The

analytical models for predicting the lip/flange distortional buckling stress of PCFS beams under pure bending have been presented in literature [20-21], in which the compressed lip and flange were selected as the object of computation (see Fig.2 (b)). It was shown that the modified Hancock's model can predict the critical stress more accurately than the modified Eurocode model. However, the computation procedure in Hancock's model was more complicated because of the use of iteration processes.

3. Analytical approaches for flange/web distortional buckling

The work by Hancock [24] indicated that when the distortional buckling was subject to pure compression, the web could be regarded as a simply supported beam (see Fig.3 (a)). When the distortional buckling was subjected to pure bending, the web could be assumed as a beam simply supported at the compression end and fixed supported at the tension end (see Fig.3(b)). Therefore, in the present study we neglect the tension flange and lip since they are fixed in the section.

Fig.4 exhibits the proposed analytical model for predicting the critical stress of flange/web distortional buckling of the PCFS beam when subjected to pure bending about the major axis. As can be seen, the model comprises the flange-lip system and the perforated web. During the flange/web distortional buckling, the perforated web will act like a plate and bend laterally. Meanwhile, the flange-lip system will follow the movement of the compression end of the perforated web and behaves like a beam retaining its original shape.

Let the compression end of the perforated web be the coordinate origin, the intersection line of the web and compression flange be the longitudinal axis (x-axis). The vertical axis (y-axis) and the lateral axis (z-axis) are set parallel to the web and flange line. The vertical and lateral displacement of the flange-lip system are denoted as w and v. The deflection of the perforated web is denoted as u. θ is the rotation of angle at the compression end of the perforated web. The height of the web, width of the flange, length of the lip and size of the hole are defined as h, b, c and d, respectively (see Fig.4).

The beam element in local coordinate system is detailed in Fig 5. The displacement and rotation of node 1 are marked as w_1 and θ_1, similarly, w_2 and θ_1 for node 2. The shape function is added to describe the deflection of the perforated web. It can be given as,

$$u = (N_{w_1} \quad N_{w_2} \quad N_{\theta_1} \quad N_{\theta_2}) \begin{pmatrix} w_1 \\ w_2 \\ \theta_1 \\ \theta_2 \end{pmatrix} \tag{1}$$

where N(y) is the Hermite interpolating function which can be expressed as follows,

$$N_{w_1} = \frac{1}{h^3}\left(2y^3 - 3hy^2 + h^3\right) \tag{2a}$$

$$N_{w_2} = -\frac{1}{h^3}\left(2y^3 - 3hy^2\right) \tag{2b}$$

$$N_{\theta_1} = \frac{1}{h^2}\left(y^3 - 2hy^2 + h^2 y\right) \tag{2c}$$

$$N_{\theta_2} = \frac{1}{h^2}\left(y^3 - hy^2\right) \tag{2d}$$

In the proposed analytical model, the tension end of the perforated web is fixed. Hence, there is no displacement or rotation in Node 2, the shape function can be simplified as follows,

$$u = N_{w_1} \cdot w_1 - N_{\theta_1} \cdot \theta_1 \tag{3}$$

The lateral displacement and rotation of the flange-lip system during flange/web distortional buckling can be assumed as follows,

$$w(x) = A_n \sum_{n=1} \sin(\frac{n\pi x}{l}) \tag{4}$$

$$\theta(x) = B_n \sum_{n=1} \sin(\frac{n\pi x}{l}) \tag{5}$$

where A_n and B_n are the constants determining the magnitude of the displacement, n is the number of half waves.

The vertical displacement of the flange-lip system is given as,

$$v = b\theta \tag{6}$$

Substituting Eq.(4) and Eq.(5) into Eq.(3), the deflection of the perforated web can be simplified as,

$$u = \frac{w}{h^3}\left(2y^3 - 3hy^2 + h^3\right) - \frac{\theta}{h^2}\left(y^3 - 2hy^2 + h^2 y\right) \tag{7}$$

According to the theory of elastic stability presented by Timoshenko[35], the strain energy of the bent perforated web is given by

$$\begin{aligned} U_{web} &= \frac{1}{2} D_1 \int_0^l \int_0^h [(\frac{\partial^2 u}{\partial x^2})^2 + (\frac{\partial^2 u}{\partial y^2})^2 + 2\mu \frac{\partial^2 u}{\partial x^2}\frac{\partial^2 u}{\partial y^2} + 2(1-\mu)(\frac{\partial^2 u}{\partial x \partial y})^2] dxdy \\ &+ \frac{1}{2}(D_2 - D_1) \int_0^l \int_{\frac{h-d}{2}}^{\frac{h+d}{2}} [(\frac{\partial^2 u}{\partial x^2})^2 + (\frac{\partial^2 u}{\partial y^2})^2 + 2\mu \frac{\partial^2 u}{\partial x^2}\frac{\partial^2 u}{\partial y^2} + 2(1-\mu)(\frac{\partial^2 u}{\partial x \partial y})^2] dxdy \end{aligned} \tag{8}$$

where D_1 is the bending stiffness of the web in solid region, D_2 is the bending stiffness of the web in perforated region, μ is the Poisson's ratio and l is the length of the beam.

Substituting Eq.(7) into Eq.(8), the strain energy of the bent perforated web can be expressed as,

$$U_{web}=\frac{D_1 l}{4}\sum_{n=1}(\frac{n\pi}{l})^2\begin{Bmatrix}[\frac{13h}{35}(\frac{n\pi}{l})^2+\frac{12}{5h}+\frac{12}{h^3}(\frac{l}{n\pi})^2]A_n^2- \\ [\frac{11h^2}{105}(\frac{n\pi}{l})^2+\frac{2+10\mu}{5}+\frac{12}{h^2}(\frac{l}{n\pi})^2]A_nB_n \\ +[\frac{h^3}{105}(\frac{n\pi}{l})^2+\frac{4h}{15}+\frac{4}{h}(\frac{l}{n\pi})^2]B_n^2\end{Bmatrix}+\frac{(D_2-D_1)l}{4}$$

$$\sum_{n=1}(\frac{n\pi}{l})^2\begin{Bmatrix}[\frac{12d^3}{h^6}(\frac{l}{n\pi})^2+\frac{d(d^6-\frac{42}{5}d^4h^2+21d^2h^4+28h^6)}{112h^6}(\frac{n\pi}{l})^2+ \\ \frac{3d^3(5h^2-d^2)}{5h^6}+2(1-\mu)\frac{3d^5-12d^3h^2+9dh^4}{4h^6}]A_n^2- \\ [\frac{12d^3}{h^5}(\frac{l}{n\pi})^2+\frac{d(d^6-\frac{28}{5}d^4h^2+\frac{7}{3}d^2h^4+14h^6)}{112h^5}(\frac{n\pi}{l})^2+ \\ \frac{10d^3h^2+5dh^4-3d^5}{5h^5}+2(1-\mu)\frac{d(3d^4-8d^2h^2+h^4)}{4h^5}]A_nB_n+ \\ [\frac{d(3d^2+h^2)}{h^4}(\frac{l}{n\pi})^2+\frac{15d^7-21d^5h^2-35d^3h^4+105dh^6}{6720h^4}(\frac{n\pi}{l})^2 \\ +\frac{-9d^5+10d^3h^2+15dh^4}{60h^4}+2(1-\mu)\frac{3d^5-2d^3h^2-dh^4}{16h^4}]B_n^2\end{Bmatrix} \tag{9}$$

It should be noted that the main effect of perforation is to reduce the flexural rigidity of the web, the property of the cross section may not change. Therefore, the position of the bending centre in proposed model is the same as the stiffened plate buckling model [32] for the CFS beam with plain web. It can be approximated as,

$$y_s=\frac{c^2}{2b+2c+h} \tag{10}$$

$$z_s=\frac{b^2+2bc}{2b+2c+h} \tag{11}$$

The strain energy of the flange-lip system due to the bending moments is given by,

$$U_{flange}=\frac{1}{2}\int_0^l[EI_y(\frac{d^2w}{dx^2})^2+EI_z(\frac{d^2v}{dx^2})^2+2EI_{yz}\frac{d^2w}{dx^2}\frac{d^2v}{dx^2}]dx+\frac{1}{2}\int_0^l GJ(\frac{d\theta}{dx})^2dx$$
$$+\frac{1}{2}\int_0^l EI_w(\frac{d^2\theta}{dx^2})^2dx \tag{12}$$

where E is the Young's modulus, I_y and I_z are the moment of inertia to bending centre about the y-axis and the z-axis, respectively. I_{yz} is the product of inertia to bending centre. G is the shear modulus. J is the torsion constant. These parameters can be determined from the following equations,

$$I_y = \frac{ct^3}{12} + ct\left(b - z_s\right)^2 + \frac{b^3 t}{12} + bt\left(\frac{b}{2} - z_s\right)^2$$

(13a)

$$I_z = \frac{c^3 t}{12} + ct\left(\frac{c}{2} - y_s\right)^2 + \frac{bt^3}{12} + bty_s^2$$

(13b)

$$I_{yz} = ct\left(\frac{c}{2} - y_s\right)\left(b - z_s\right) - bty_s\left(\frac{b}{2} - z_s\right)$$

(13c)

$$J = \frac{\left(b + c\right)t^3}{3}$$

(13d)

$$I_\omega = 0$$

(13e)

Substituting Eq.(4), Eq.(5) and Eq.(6) into Eq.(12), the strain energy of the flange-lip system can be expressed as,

$$U_{flange} = \frac{El}{4}\sum_{n=1}(\frac{n\pi}{l})^4[A_n^2 I_y + B_n^2 b^2 I_z + 2A_n B_n b I_{yz} + (\frac{GJ}{E})(\frac{l}{n\pi})^2 B_n^2]$$

(14)

Note that, in the present model the perforated web and the compressed flange-lip are modeled together as a whole system, and thus the web will also rotate about the bending center while the flange deforms. To satisfy the deformation compatibility condition, the additional strain energy of the perforated web deformed as a stiffener needs to be taken into account, which can be expressed as follows,

$$U_1 = \frac{t_1}{2}\int_0^l\int_0^h Ez_s^2\frac{y^2}{h^2}(\frac{\partial^2 w}{\partial x^2})^2\,dxdy - \frac{t_2}{2}\int_0^l\int_{\frac{h-d}{2}}^{\frac{h+d}{2}} Ez_s^2\frac{y^2}{h^2}(\frac{\partial^2 w}{\partial x^2})^2\,dxdy$$

(15)

$$U_2 = \frac{t_1}{2}\int_0^l\int_0^h Ey_s^2\frac{y^2}{h^2}(\frac{\partial^2 v}{\partial x^2})^2\,dxdy - \frac{t_2}{2}\int_0^l\int_{\frac{h-d}{2}}^{\frac{h+d}{2}} Ey_s^2\frac{y^2}{h^2}(\frac{\partial^2 v}{\partial x^2})^2\,dxdy$$

(16)

where t_1 is the thickness of the web in solid region, t_2 is the reduced thickness of the web in perforated region which takes into account the effect of web openings (holes).

Substituting Eqs.(4), (5) and (6) into Eqs.(15) and (16), it yields,

$$U_1 = \sum_{n=1}(\frac{n\pi}{l})^4\frac{Elt_1}{12}hA_n^2 z_s^2 - \sum_{n=1}(\frac{n\pi}{l})^4\frac{Elt_2}{12}\frac{d(d^2+3h^2)}{4h^2}A_n^2 z_s^2$$

(17)

$$U_2 = \sum_{n=1} (\frac{n\pi}{l})^4 \frac{Elt_1}{12} hb^2 B_n^2 y_s^2 - \sum_{n=1} (\frac{n\pi}{l})^4 \frac{Elt_2}{12} \frac{d(d^2+3h^2)}{4h^2} b^2 B_n^2 y_s^2$$

(18)

The external work done by the pre-buckling axial stress in the perforated web and flange-lip system can be established as,

$$W_{web} = \frac{1}{2}\sigma_{cr} t \int_0^l \int_0^h (-\frac{2y}{h}+1) \frac{\partial^2 u}{\partial x^2} dydx \tag{19}$$

$$W_{flange} = \frac{1}{2}\sigma_{cr} t \int_0^l \int_0^b [(\frac{dw}{dx})^2 + (z\frac{d\theta}{dx})^2] dzdx + \frac{1}{2}\sigma_{cr} t \int_0^l \int_0^c [(\frac{dw}{dx} - y\frac{d\theta}{dx})^2 + (\frac{dv}{dx})^2] dydx \tag{20}$$

where σ_{cr} is the critical stress of the flange/web distortional buckling.

Substituting Eqs.(3)-(6) into Eqs.(19) and (20), it yields,

$$W_{web} = \frac{1}{4}\sigma_{cr} tl \sum_{n=1} (\frac{n\pi}{l})^2 (\frac{h}{5} A_n^2 - \frac{4h^2}{105} A_n B_n + \frac{h^3}{420} B_n^2) \tag{21}$$

$$W_{flange} = \frac{1}{4}\sigma_{cr} tl \sum_{n=1} (\frac{n\pi}{l})^2 [(b+c)A_n^2 - c^2 A_n B_n + (\frac{1}{3}b^3 + b^2 c + \frac{1}{3}c^3) B_n^2] \tag{22}$$

According to the principle of minimum potential energy, the total potential energy of the system will have a stationary condition with respect to the constants A_n and B_n when the flange/web distortional buckling happens. This gives as,

$$\frac{\partial \Pi}{\partial A_n} = \frac{\partial}{\partial A_n}\left(U_{\text{web}} + U_{\text{flange}} + U_1 + U_2 - W_{\text{web}} - W_{\text{flange}}\right) = 0 \tag{23}$$

$$\frac{\partial \Pi}{\partial B_n} = \frac{\partial}{\partial B_n}\left(U_{\text{web}} + U_{\text{flange}} + U_1 + U_2 - W_{\text{web}} - W_{\text{flange}}\right) = 0 \tag{24}$$

The Rayleigh-Ritz method is utilized to solve the eigenvalue problems. The simultaneous equations can be re-written as,

$$\left\{ \begin{bmatrix} a_{11} & a_{12} \\ a_{21} & a_{22} \end{bmatrix} - \sigma_{\text{cr}} t \begin{bmatrix} b_{11} & b_{12} \\ b_{21} & b_{22} \end{bmatrix} \right\} \begin{Bmatrix} A_n \\ B_n \end{Bmatrix} = \begin{Bmatrix} 0 \\ 0 \end{Bmatrix} \tag{25}$$

where a_{ii} and b_{jj} are the coefficients of simultaneous equations which can be given by,

$$a_{11}=D_1\left[\frac{13h}{35}(\frac{n\pi}{l})^2+\frac{12}{5h}+\frac{12}{h^3}(\frac{l}{n\pi})^2\right]+(D_2-D_1)$$
$$\left[\begin{array}{l}\frac{12d^3}{h^6}(\frac{l}{n\pi})^2+\frac{d(d^6-\frac{42}{5}d^4h^2+21d^2h^4+28h^6)}{112h^6}(\frac{n\pi}{l})^2\\+\frac{3d^3(5h^2-d^2)}{5h^6}+2(1-\mu)\frac{3d^5-12d^3h^2+9dh^4}{4h^6}\end{array}\right]$$
$$+E\left(\frac{n\pi}{l}\right)^2[I_y+\frac{ht_1z_s^2}{3}-\frac{z_s^2dt_2(d^2+3h^2)}{12h^2}]$$

$$a_{12}=a_{21}=-D_1\left[\frac{11h^2}{210}(\frac{n\pi}{l})^2+\frac{1+5\mu}{5}+\frac{6}{h^2}(\frac{l}{n\pi})^2\right]-(D_2-D_1)$$
$$\left[\begin{array}{l}\frac{6d^3}{h^5}(\frac{l}{n\pi})^2+\frac{d(d^6-\frac{28}{5}d^4h^2+\frac{7}{3}d^2h^4+14h^6)}{224h^5}(\frac{n\pi}{l})^2+\\\frac{10d^3h^2+5dh^4-3d^5}{10h^5}+(1-\mu)\frac{d(3d^4-8d^2h^2+h^4)}{4h^5}\end{array}\right]$$
$$+\mathrm{b}E\left(\frac{n\pi}{l}\right)^2I_{yz}$$

$$a_{22}=D_1\left[\frac{h^3}{105}(\frac{n\pi}{l})^2+\frac{4h}{15}+\frac{4}{h}(\frac{l}{n\pi})^2\right]+(D_2-D_1)$$
$$\left[\begin{array}{l}\frac{d(3d^2+h^2)}{h^4}(\frac{l}{n\pi})^2+\frac{15d^7-21d^5h^2-35d^3h^4+105dh^6}{6720h^4}(\frac{n\pi}{l})^2\\+\frac{-9d^5+10d^3h^2+15dh^4}{60h^4}+2(1-\mu)\frac{3d^5-2d^3h^2-dh^4}{16h^4}\end{array}\right]$$
$$+b^2E\left(\frac{n\pi}{l}\right)^2\left(I_z+\frac{ht_1y_s^2}{3}-\frac{y_s^2dt_2(d^2+3h^2)}{12h^2}\right)+GJ$$

$$b_{11}=\frac{h}{5}+b+c$$

$$b_{12}=b_{21}=-\frac{2h^2}{105}-\frac{c^2}{2}$$

$$b_{22}=\frac{h^3}{420}+\frac{b^3+3\mathrm{b}^2c+c^3}{3}$$

The eigenvalue equation Eq.(25) can be solved by the numerical calculation software Matlab, in which the smallest eigenvalue is selected as the critical stress of flange/web distortional buckling of PCFS beams. Furthermore, *l*/*n* represents the half-wave length of the buckling mode. The novel point in this paper is that the calculation procedure does not need iteration which can improve the computation efficiency.

4. Finite element analysis and validation

To validate the result of the proposed analytical model, the flange/web distortional buckling behaviour was examined with eigen-buckling analyses by using the finite element analysis software ANSYS. A total of 140 specimens selected from Albion section with various hole sizes and beam lengths were analysed. The location and dimension of the openings were shown in Fig.6. For convenience, the distance between the two holes was set $\pi d/2$ which indicated that the area of openings was half of the area of perforated region. Hence, the concept of equivalent thickness could be applied for determining the reduce of thickness and bending stiffness of the perforated web. In this case, the thickness of the perforated region was half of the solid region (t_2=0.5t_1), the equivalent plate-type bending stiffness of the perforated region was one eighth of that of the solid region (D_2=0.125D_1).

The element used in numerical study was four-node isoparametric thin shell 181 element with six degrees of freedom. The material properties of the PCFS beams were assumed as E=205 GPa, μ=0.3 and σ_y=390 MPa. The cross-section dimension of each specimen selected from Albion section was given in Table 1. The maximum mesh size was taken not exceeding 10 mm which can satisfy the requirement of precision.

The loading and boundary conditions of the PCFS beams could be observed in Fig.7. Based on the equivalent theory of statics, the node forces applied at the web and lips were linearly distributed whereas at the flanges are uniformly distributed to simulate the pure bending. The PCFS beams were simply supported at its two ends. Therefore, the translations of the end nodes in the x and y directions were restrained, the rotation of the end nodes about the z direction was also restrained. To avoid the rigid displacement in longitudinal direction, the translation of Point A in the z direction was restrained. Furthermore, the rotation of the web tension end about the z-axis was also restrained in present study.

The flange/web distortional buckling curves of the PCFS beams subject to pure bending produced by eigenvalue analyses were displaced in Fig. 8, in which σ_{cr} was the flange/web distortional buckling stress, σ_y was the yield stress of the beam. Three different section sizes having web height of 120 mm, 200 mm and 300 mm were selected from Albion section representing small, medium and large sections. The diameter of circular hole was in the range of 25%-50% of the web height. It can be seen that all the curves had the similar tendency, the local minimum point was the critical stress of flange/web distortional buckling. The critical stresses decreased as the diameter of circular hole increased. The typical flange/web distortional buckling modes with one, two and three half waves were detailed in Fig.9.

Note that the finite strip software CUFSM [2] uses the strip elements which does not have the function to model the web openings and thus cannot be used to calculate the critical buckling stress of PCFS beams. Comparisons of critical stresses of flange/web distortional buckllling of CFS beams with no holes in the web obtained from ANSYS and CUFSM were made as shown in Table 2. For the finite element model with plain web, the parameters including loading conditions, boundary conditions, mesh sizes, material properties were the same with the model with web holes. It can be observed from Table 2 that the maximum gap between the results obtained from ANSYS and

CUFSM was no more than 8% which indicated a good accuracy of the finite element model.

The comparison of critical stresses of flange/web distortional buckling of the PCFS beams between the proposed analytical model and FEA for three typical sections and Section 2 with different hole sizes were given in Fig.10 and Fig.11, respectively. The line represented the result calculated from Eq.(25) and the point represented the result obtained from FEA. The data in the figures indicated that the proposed analytical model was more conservative when the beam length was longer than one half-wave length of the buckling mode. This was primarily because the shape function in the proposed analytical method involves only the sine-functions, which are probably oversimplified. Nevertheless, all the lowest critical stresses could match the data obtained from FEA well which revealed that the proposed analytical model could be utilized into the design specifications.

The parametric study was listed in Fig.12, for which all the sections analyzed were picked from Table 1. The lowest critical stresses obtained from the proposed analytical model and FEA were used for comparison, in which the beams with large openings (d/h=0.5) and small openings (d/h=0.25) could be found in Fig.12(a) and Fig.12(b), respectively. As we can see from the figures, the result obtained from the proposed model showed a good agreement with FEA result in all cases. The comparisons of critical stresses of flange/web distortional buckling of PCFS beams between numerical and theoretical investigations were shown in Table 3, which gives the mean value of the $\sigma_{cr,an}/\sigma_{cr,FEA}$ ratio for the beam with d/h=0.5 and 0.25 to be 0.990 and 0.998 with the corresponding coefficient of variation (COV) 0.0158 and 0.0161, respectively.

This proved that the presented model could capture the main characteristics of flange/web distortional buckling of the PCFS beams well.

5. Conclusions

This paper has presented a study on the flange/web distortional buckling of PCFS beams. By means of the classical energy principle (Ritz method) an analytical approximate expression for calculating the critical stress of flange/web distortional buckling of PCFS beams with circular holes in the web when subjected to pure bending is derived. The present analytical solution has been validated by using the finite element analysis method. From the results obtained the following conclusions can be drawn.

- The web openings can reduce the flexural rigidity of the web and thus decrease the resistance of the beam to the distortional buckling of the flange-lip system.
- The concept of equivalent thickness can be applied for determining the reduction of web thickness and corresponding bending stiffness of the perforated web.
- In characterizing flange/web distortional buckling, the compressed flange-lip can be treated as a beam and the perforated web can be regarded as a plate. Hermite interpolating shape functions can be used to describe the deformation of the perforated web while buckling occurs.

- There is a good agreement between the proposed analytical model and the FEA, indicating that the present model is appropriate and reliable and could be extended into the design specifications for the PCFS beams.

Acknowledgements

The authors are grateful to the financial support from the Natural Science Foundation of Zhejiang Province (No.LY19E080020). The first author would like to acknowledge the studentship supported by the China Scholarship Council (No. 201708330276).

References

[1] C.D. Moen and B.W. Schafer (2009): Elastic buckling of cold-formed steel columns and beams with holes. Engineering Structures, 31, 2812-2824.

[2] B.W. Schafer and S. Ádány (2006): Buckling analysis of cold-formed steel members using CUFSM: conventional and constrained finite strip methods. (CUFSM Version 2.6). Eighteenth International Specialty Conference on Cold-Formed Steel Structures, Orlando, Florida, USA: October 26&27.

[3] F.H. Smith and C.D. Moen (2014): Finite strip elastic buckling solution for thin-walled metal columns with perforations. Thin-walled Structures, 79, 187-201.

[4] T.C.H. Liu and K.F. Chung (2003): Steel beams with large web openings of various shapes and sizes: finite element investigation. Journal of Constructional Steel Research, 59, 1159-1176.

[5] V.V. Degtyarev and N.V. Degtyareva (2017): Numerical simulations on cold-formed steel channels with flat slotted webs in shear. Part I: Elastic shear buckling characteristics. Thin-walled Structures, 119, 22-32.

[6] V.V. Degtyarev and N.V. Degtyareva (2017): Numerical simulations on cold-formed steel channels with flat slotted webs in shear. Part II: Ultimate shear strength. Thin-walled Structures, 119, 211-223.

[7] S.H. Pham, C.H. Pham and G.J. Hancock (2017): Direct strength method of design for channel sections in shear with square and circular web holes. Journal of Structural Engineering ,143(6): 0417017.

[8] C.D. Moen and B.W. Schafer (2008): Experiments on cold-formed steel columns with holes. Thin-walled Structures, 46, 1164-1182.

[9] A. Crisan, V. Ungureanu and D. Dubina (2012): Behaviour of cold-formed steel perforated sections in compression. Part 1-Experimental investigations. Thin-walled Structures, 61, 86-96.

[10] M.P. Kulatunga and M. Macdonald (2013): Investigation of cold-formed steel structural members with perforations of different arrangements subject to compression loading. Thin-walled Structures, 67, 78-87.

[11] M.P. Kulatunga, M. Macdonald, J. Rhodes and D.K. Harrison (2014): Load capacity of cold-formed column members of lipped channel cross-section with perforations subjected to compression. Thin-walled Structures, 80, 1-12.

[12] R.M. Lawson and A. Basta (2019): Deflection of C section beam with circular web openings. Thin-walled Structures, 134, 277-290.

[13] A. Uzzaman, J.B.P. Lim, D. Nash and B. Young (2017): Effects of edge-stiffened circular holes on the web crippling strength of cold-formed steel channel sections under one-flange loading conditions. Engineering Structures, 139, 96-107.

[14] A. Uzzaman, J.B.P. Lim, D. Nash and K. Roy (2020): Web crippling behaviour of cold-formed steel channel sections with edge-stiffened and unstiffened circular holes under interior-two-flange loading condition. Thin-walled Structures, 154, 106813.

[15] A. Uzzaman, J.B.P. Lim, D. Nash and K. Roy (2020): Cold-formed steel channel sections under end-two-flange loading condition: Design for edge-stiffened holes, unstiffened holes and plain webs. Thin-walled Structures, 147, 106532.

[16] B.S. Chen, K. Roy, A. Uzzaman, G.M. Raftery, D. Nash, G.C. Clifton, P. Pouladi and J.B.P. Lim (2019): Effects of edge-stiffened web openings on the behaviour of cold-formed steel channel sections under compression. Thin-walled Structures, 144, 106307.

[17] B.S. Chen, K. Roy, A. Uzzaman, G.M. Raftery and J.B.P. Lim (2020): Parametric study and simplified design equations for cold-formed steel channels with edge-stiffened holes under axial compression. Journal of Constructional Steel Research, 172, 106161.

[18] B.S. Chen, K. Roy, A. Uzzaman and J.B.P. Lim (2020): Moment capacity of cold-formed steel channels with edge-stiffened holes, un-stiffened holes and plain webs. Thin-walled Structures, 157, 107070.

[19] B.S. Chen, K. Roy, A. Uzzaman, G. Raftery and J.B.P. Lim (2020): Axial strength of back-to-back cold-formed steel channels with edge-stiffened holes, un-stiffened holes and plain webs. Journal of Constructional Steel Research, 174, 106313.

[20] W.B. Yuan, N.T. Yu and L.Y. Li (2017): Distortional buckling of perforated cold-formed steel channel-section beams with circular holes in web. International Journal of Mechanical Sciences, 126, 255-260.

[21] N.T. Yu, B. Kim, W.B. Yuan, L.Y. Li and F. Yu (2019): An analytical solution of distortional buckling resistance of cold-formed steel channel-section beams with web openings. Thin-Walled Structures, 135, 446-452.

[22] N.T. Yu, B. Kim, L.Y. Li, W.J. Hong and W.B. Yuan (2020): Distortional buckling of perforated cold-formed steel beams subject to uniformly distributed transverse loads. Thin-Walled Structures, 148, 106569.

[23] S.C.W. Lau and G.J. Hancock (1987): Distortional buckling formulas for channel columns. Journal of Structural Engineering, 113(5), 1063-1078.

[24] G.J. Hancock (1997): Design for distortional buckling of flexural members. Thin-Walled Structures, 27(1), 3-12.

[25] EN1993-1-3. Eurocode 3–Design of steel structures–Part 1-3: General rules–Supplementary rules for cold-formed members and sheeting, BSI; 2006.

[26] H. Mousavi, M. Azhari, M. M. Saadatpour and S. Sarrami-Foroushani (2020): Application of improved element-free Galerkin combining with finite strip method for buckling analysis of channel-section beams with openings. Engineering with computers, DOI: 10.1007/s00366-020-01087-8.

[27] L.Y. Li and J.K. Chen (2008): An analytical model for analysing distortional buckling of cold-formed steel sections. Thin-walled Structures, 46(12), 1430-1436.

[28] C.A. Rogers and R.M. Schuster (1997): Flange/web distortional buckling of cold-formed steel sections in bending. Thin-Walled Structures, 27(1), 13-29.

[29] G.J. Hancock (2003): Cold-formed steel structures. Journal of Constructional Steel Research, 59(4), 473-487.

[30] A.B. Badawy Abu-Sena, J.C. Chapman and P.C. Davidson (2001): Interaction between critical torsional flexural and lip buckling in channel sections. Journal of Constructional Steel Research, 57(8), 925-944.

[31] W.B. Yuan, S.S. Cheng, L.Y. Li and B. Kim (2014): Web-flange distortional buckling of partially restrained cold-formed steel purlins under uplift loading. International Journal of Mechanical Science, 89, 476-481.

[32] J. Zhu and L.Y. Li (2016): A stiffened plate buckling model for calculating critical stress of distortional buckling of CFS beams. International Journal of Mechanical Sciences, 115-116, 457-464.

[33] X.H. Huang and J. Zhu (2016): A stiffened-plate buckling model for calculating critical stress of distortional buckling of CFS columns. International Journal of Mechanical Science, 119, 237-242.

[34] X.H. Huang, J. Yang, Q.F. Liu, J. Zhu, L. Bai, F.L. Wang and J.H. Wang (2018): A simplified flange-lip model for distortional buckling of cold-formed steel channel-sections with stiffened web. International Journal of Mechanical Science, 136, 451-459.

[35] S.P. Timoshenko and J.M. Gere (1961): Theory of elastic stability. New York: McGraw Hill, US

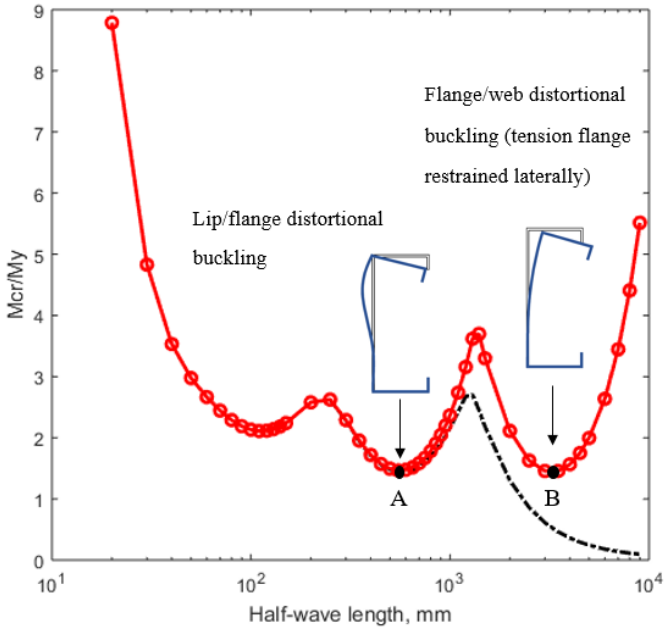

Fig.1 Buckling curve of cold-formed steel sections in pure bending (curve produced by CUFSM [2])

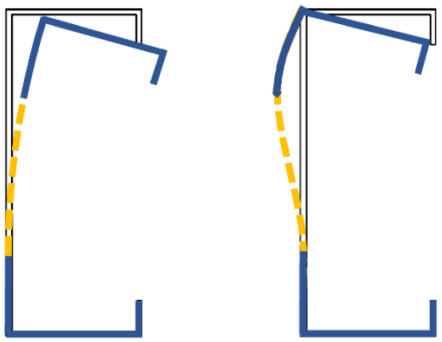

(a) (b)

Fig.2 Distortional buckling modes of PCFS beams (a) Flange/web distortional buckling (b) Lip/flange distortional buckling

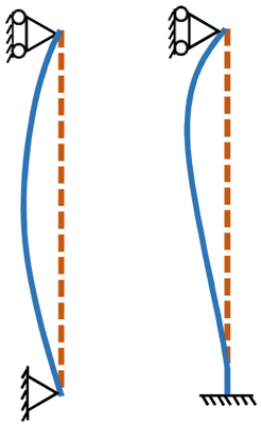

(a) (b)

Fig.3 Web deformation of the CFS sections due to the distortional buckling (a) pure compression (b) pure bending

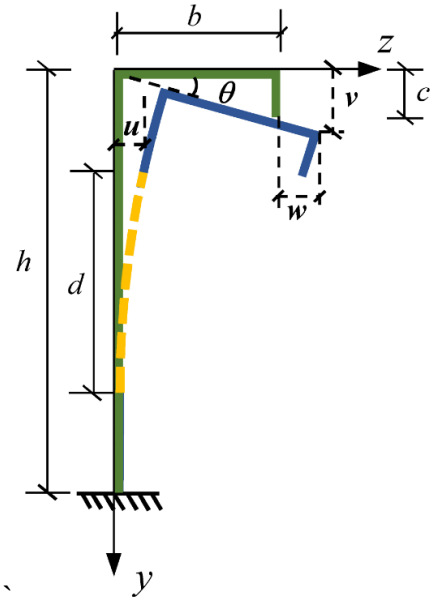

Fig.4 Analytical model for flange/web distortional buckling of the PCFS beam subject to pure bending

Fig.5 Beam element in local coordinate system

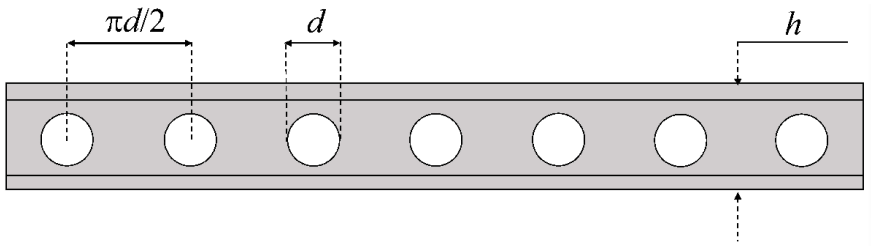

Fig.6 Location and dimension of the openings

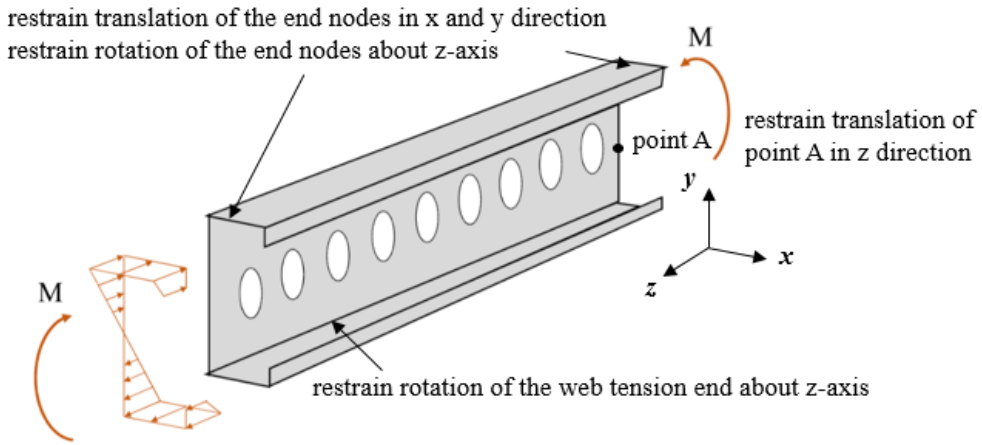

Fig.7 Loading and boundary conditions of the PCFS beams

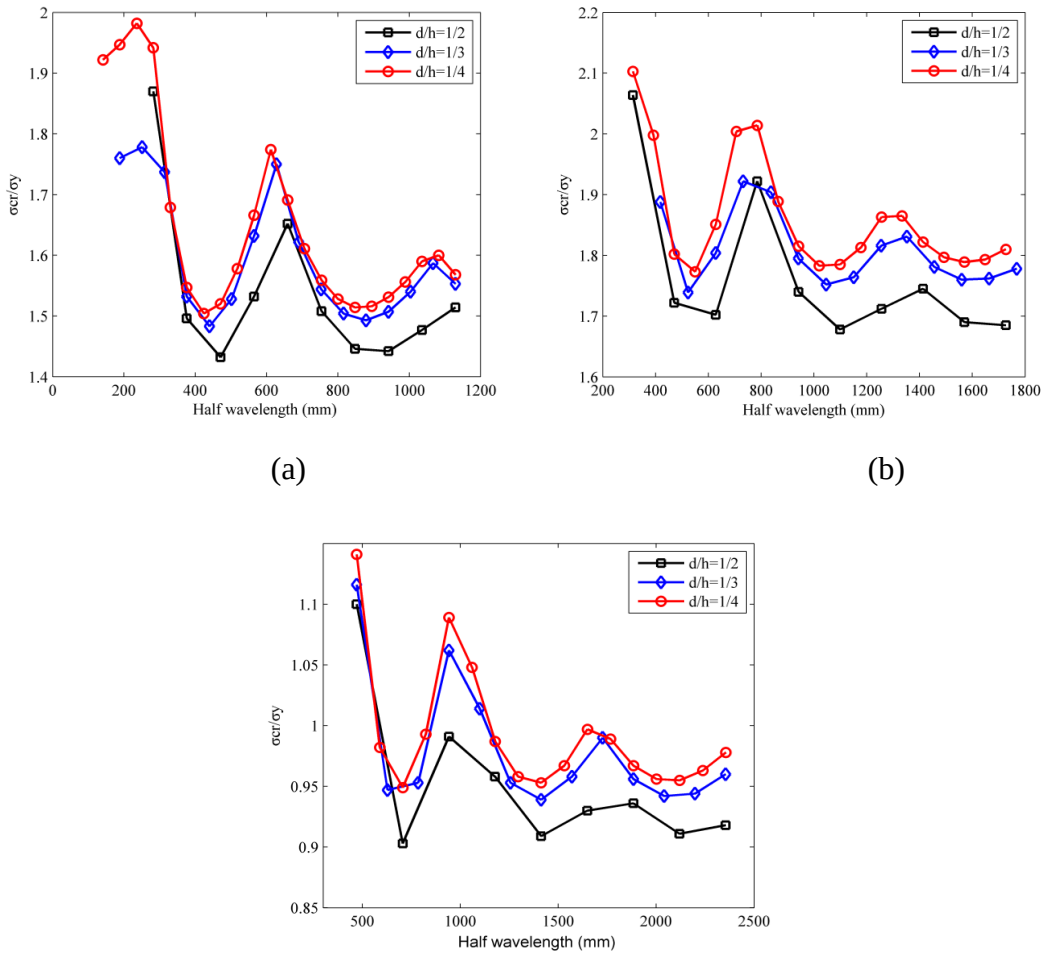

Fig.8 Flange/web distortional buckling curves of the PCFS beams subject to pure bending (a) Section 1: h=120 mm, b=50 mm, c=15 mm, t=1.5 mm (b) Section 2: h=200 mm, b=65 mm, c=20 mm, t=2.5 mm (c) Section 3: h=300 mm, b=100 mm, c=20 mm, t=3 mm (curves produced by ANSYS, σ_y=390 MPa)

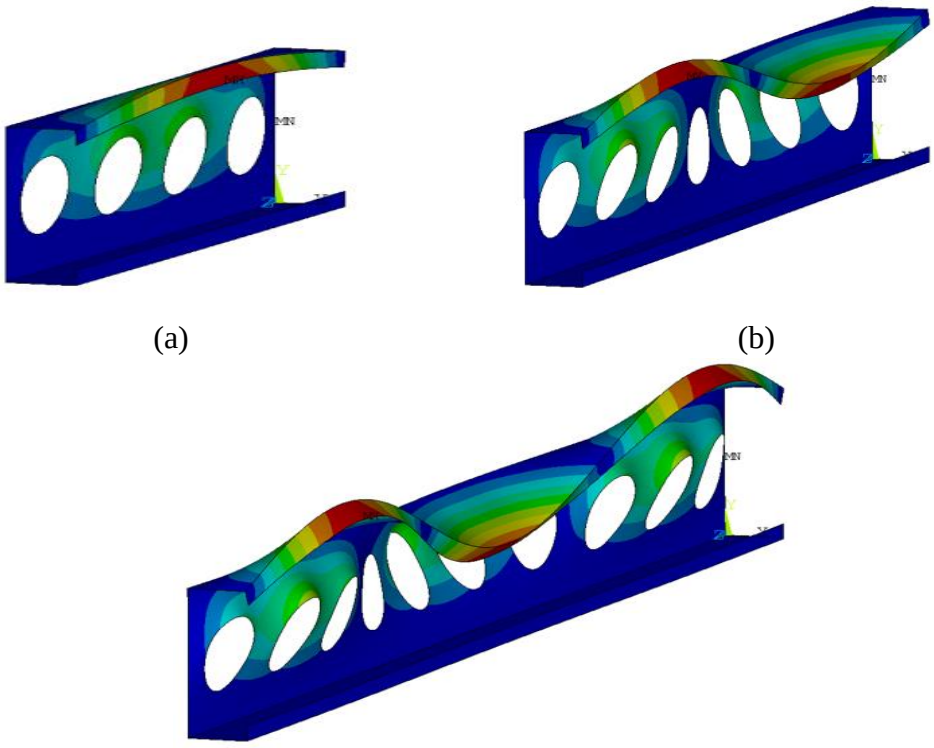

(a) (b)

(c)

Fig.9 Typical flange/web distortional buckling modes of the PCFS beam in the ANSYS Eigen-buckling analyses (a) one half wave, l=628 mm (b) two half waves, l= 1099 mm (c) three half waves, l=1570 mm (Section2: h=200 mm, b=65 mm, c=20 mm, t=2.5 mm, d=100 mm)

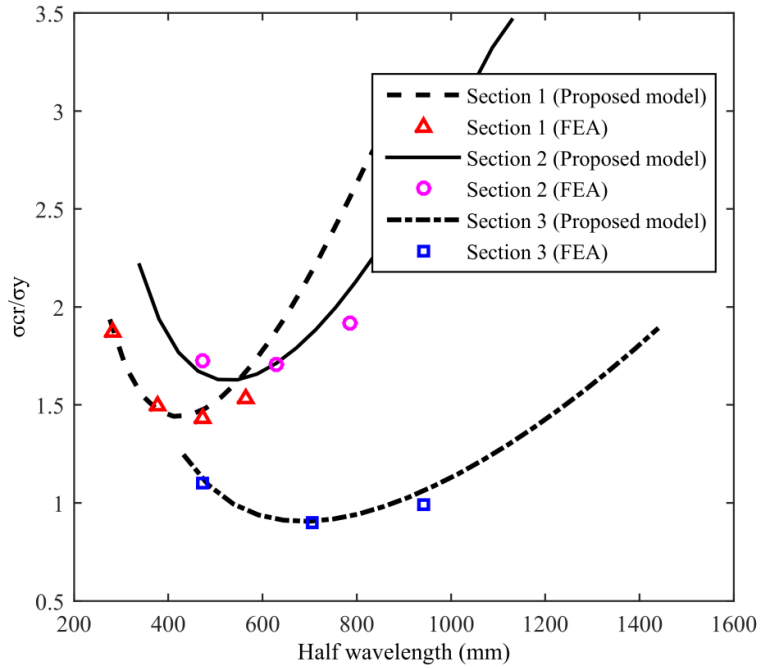

Fig.10 Critical stresses of flange/web distortional buckling of the PCFS beams with different sections (Section 1: h=120 mm, b=50 mm, c=15 mm, t=1.5 mm, d=60 mm; Section 2: h=200 mm, b=65 mm, c=20 mm, t=2.5 mm, d=100 mm; Section 3: h=300 mm, b=100 mm, c=20 mm, t=3 mm, d=150 mm)

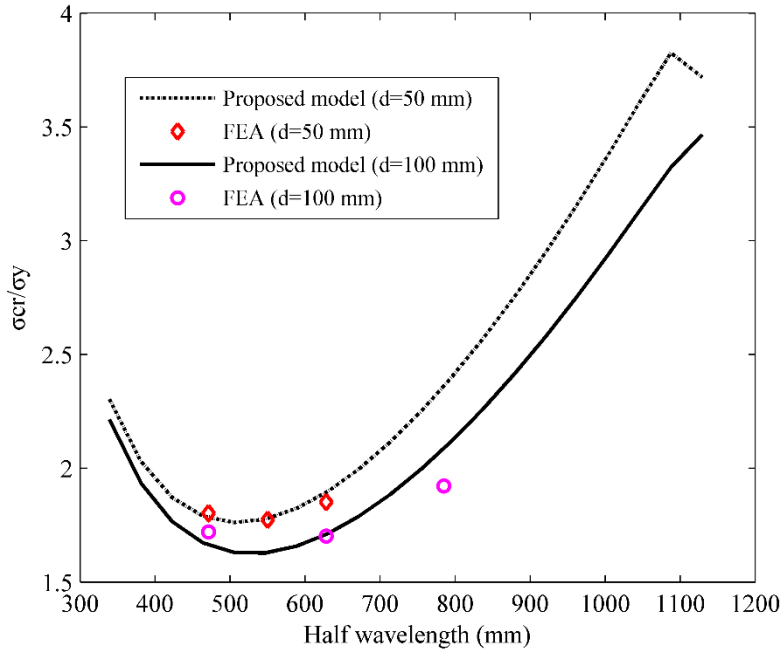

Fig.11 Critical stresses of flange/web distortional buckling of the PCFS beams with different hole sizes (Section 2: h=200 mm, b=65 mm, c=20 mm, t=2.5 mm)

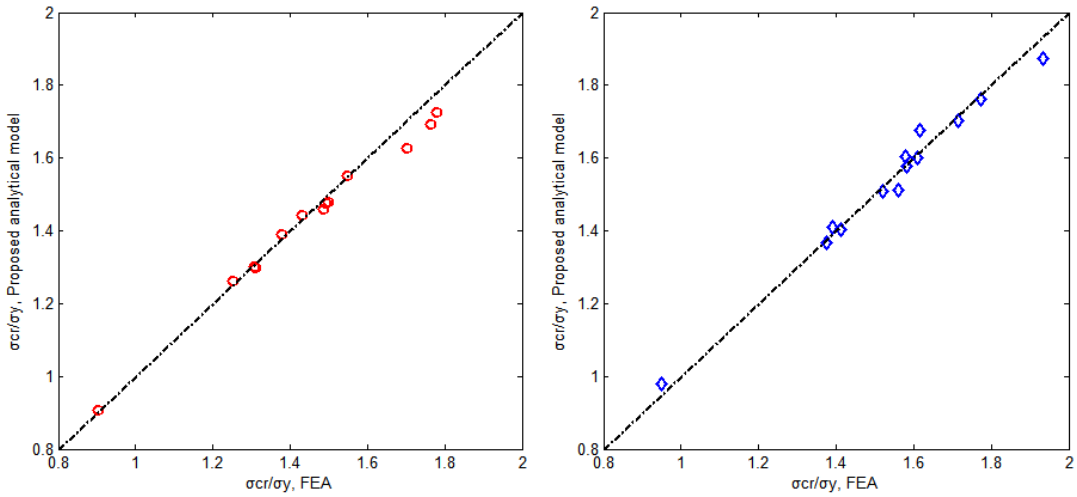

(a) (b)

Fig.12 Comparison of critical stresses of flange/web distortional buckling of the PCFS beams between the proposed model and FEA (a) d/h=0.5 (b) d/h=0.25 (PCFS sections are selected from Albion section)

Table 1 Typical dimension of the PCFS section selected from Albion section in UK

Specimen	Web, h (mm)	Flange, b (mm)	Lip, c (mm)	Thickness, t (mm)
C12515	120	50	15	1.5
C12516	120	50	15	1.6
C14616	145	62.5	20	1.6
C14618	145	62.5	20	1.8
C17618	175	62.5	20	1.8
C17620	175	62.5	20	2.0
C20620	200	65	20	2.0
C20625	200	65	20	2.5
C22625	225	65	20	2.5
C24625	240	65	20	2.5
C24630	240	65	20	3.0
C26630	265	65	20	3.0
C30730	300	75	20	3.0

Table 2 Comparisons of critical stresses of flange/web distortional buckllling of CFS beams with no holes in the web obtained from ANSYS and CUFSM (Section 2: h=200 mm, b=65 mm, c=20 mm, t=2.5 mm)

Length l (mm)	Critical stress obtained from ANSYS $\sigma_{cr,\,ANSYS}$ (MPa)	Critical stress obtained from CUFSM $\sigma_{cr,\,CUFSM}$ (MPa)	Comparison $\sigma_{cr,ANSYS}/\sigma_{cr,CUFSM}$
400	791.7	856.2	0.92
450	739.5	795.9	0.93
500	781.5	769.0	0.93
550	720.5	767.0	0.94
600	740.1	784.0	0.94
650	773.5	815.8	0.95
700	817.9	859.6	0.95

Table 3 Comparison of critical stresses of flange/web distortional buckling of PCFS beams between numerical and theoretical investigations

Specimen	Critical stress obtained from proposed method $\sigma_{cr,an}$ (MPa)		Critical stress obtained from FEA $\sigma_{cr,FEA}$ (MPa)		Comparison	
					$\sigma_{cr,an}/\sigma_{cr,FEA}$	$\sigma_{cr,an}/\sigma_{cr,FEA}$
	d/h=0.5	d/h=0.25	d/h=0.5	d/h=0.25	d/h=0.5	d/h=0.25
C12515	562.3	589.6	558.6	608.6	1.01	0.97
C12516	605.1	605.1	604.1	604.1	1.00	1.00
C14616	507.0	549.9	510.4	541.9	0.99	1.01
C14618	576.3	624.9	584.4	615.7	0.99	1.02
C17618	506.1	547.8	510.8	550.3	0.99	1.00
C17620	568.9	615.8	580.2	617.3	0.98	1.00
C20620	492.6	533.1	488.6	536.0	1.01	0.99
C20625	635.0	687.3	663.7	691.4	0.96	0.99
C22625	575.1	623.8	582.4	628.2	0.99	0.99
C24625	541.8	588.4	537.3	592.8	1.01	0.99
C24630	672.7	731.0	694.3	754.6	0.97	0.97
C26630	609.8	664.1	626.1	668.9	0.97	0.99
C30730	353.3	381.7	352.3	370.9	1.00	1.03

Notations

CFS	cold-formed steel
PCFS	perforated cold-formed steel
w	vertical displacement of the flange-lip system
v	lateral displacement of the flange-lip system
u	deflection of the perforated web
θ	rotation of angle at the compression end of the perforated web
h	height of the web
b	width of the flange
c	length of the lip
d	diameter of the hole
D_1	bending stiffness of the web in solid region
D_2	bending stiffness of the web in perforated region
μ	Poisson's ratio
l	length of the beam
E	Young's modulus
I_y	moment of inertia to shear center about the y-axis
I_z	moment of inertia to shear center about the z-axis
I_{yz}	product of inertia to shear center
G	shear modulus
J	torsion constant
U_{web}	strain energy of the bent perforated web
U_{flange}	strain energy of the flange-lip system
W_{web}	external work done by the pre-buckling axial stress in the perforated web
W_{flange}	external work done by the pre-buckling axial stress in the flange-lip system
t_1	thickness of the web in solid region
t_2	thickness of the web in perforated region
σ_{cr}	critical stress of the flange/web distortional buckling
n	number of halfwave